

Sensitivity estimate of proposed searches for exotic spin-dependent interactions using polarized helium

P.-H. Chu,* Y. J. Kim,† and I. Savukov

Los Alamos National Laboratory, Los Alamos, New Mexico 87545, USA

(Dated: March 4, 2020)

We investigate the sensitivities of searches for exotic spin-dependent interactions between the polarized nuclear spins of ^3He and the particles of unpolarized or polarized solid-state masses using the frequency method and the resonance method. In the frequency method, the spin-dependent interactions act as an effective static magnetic field, causing the frequency shift to the spin precession of ^3He . In the resonance method, proposed by Arvanitaki and Geraci [Phys. Rev. Lett. 113, 161801 (2014)] for the significant improvement of the experimental sensitivities on the spin-dependent interactions, the mass movement is modulated at the Larmor frequency of ^3He . This results in the modulating spin-dependent interactions inducing an effective oscillatory magnetic field, which can tilt the ^3He spins, similarly as an oscillatory magnetic field in nuclear magnetic resonance. We estimate the sensitivities of the searches using a room-temperature ^3He target for its extremely long relaxation time. New limits on the coupling strengths of the spin-dependent interactions can be set in the interaction length range below 10^{-1} m.

Since the discovery of intrinsic spin [1], exotic spin-dependent interactions between fermions have been of interest. Moody and Wilczek [2] first considered some types of exotic interactions between polarized spins and unpolarized or polarized particles through new spin-0 boson exchange. Later, Dobrescu and Mocioiu [3] extended this idea by including the operators dependent on the relative velocity between two interacting particles in the non-relativistic limit through new spin-1 boson exchange. Recently, these exotic spin-dependent interactions have attracted people's attention because they are observables of new spin-0 or spin-1 bosons, which may solve several mysteries in fundamental physics. For example, the axion as a spin-0 boson was introduced in the theory to explain the lack of charge-parity (CP) violation in the strong interaction [4] and the cold dark matter [5]. Several theoretical concepts including string theory [6], hierarchy problem [7], dark energy [8], unparticles [9], dark photons [10–12] also predict the existence of such new bosons. A review article describing the recent theoretical progress in this field can be found in Ref. [13].

There are fifteen possible exotic spin-dependent interactions described in Ref. [3], which have been revisited in a convenient format [14, 15]. The contact terms have been also studied for the superficial singularity [15, 16]. In this paper we still use the fifteen interaction formats adopting the numbering scheme in Ref. [3] since we will not consider the contact term. In a system of two particles (particle 1, 2 are fermions like electrons, neutrons, protons, etc.) with spin 1 ($\hat{\sigma}_1$) and 2 ($\hat{\sigma}_2$), and mass 1 (m_1) and 2 (m_2) respectively, their relative distance and relative velocity are \vec{r} and \vec{v} . We can group the spin-dependent interactions between these two particles as static spin-dependent interactions, spin-velocity-dependent interactions and spin-

velocity-velocity-dependent interactions. The group one includes the interactions:

$$V_2 = f_2 \frac{\hbar c}{4\pi} (\hat{\sigma}_1 \cdot \hat{\sigma}_2) \left(\frac{1}{r} \right) e^{-r/\lambda}, \quad (1)$$

$$V_3 = f_3 \frac{\hbar^3}{4\pi m_1 m_2 c} \left[(\hat{\sigma}_1 \cdot \hat{\sigma}_2) \left(\frac{1}{\lambda r^2} + \frac{1}{r^3} \right) - (\hat{\sigma}_1 \cdot \hat{r})(\hat{\sigma}_2 \cdot \hat{r}) \left(\frac{1}{\lambda^2 r} + \frac{3}{\lambda r^2} + \frac{3}{r^3} \right) \right] e^{-r/\lambda}, \quad (2)$$

$$V_{9+10} = f_{9+10} \frac{\hbar^2}{8\pi m_1} (\hat{\sigma}_1 \cdot \hat{r}) \left(\frac{1}{\lambda r} + \frac{1}{r^2} \right) e^{-r/\lambda}, \quad (3)$$

$$V_{11} = -f_{11} \frac{\hbar^2}{4\pi m_\mu} [(\hat{\sigma}_1 \times \hat{\sigma}_2) \cdot \hat{r}] \left(\frac{1}{\lambda r} + \frac{1}{r^2} \right) e^{-r/\lambda} \quad (4)$$

The group two includes the interactions:

$$V_{4+5} = -f_{4+5} \frac{\hbar^2}{8\pi m_1 c} [\hat{\sigma}_1 \cdot (\vec{v} \times \hat{r})] \times \left(\frac{1}{\lambda r} + \frac{1}{r^2} \right) e^{-r/\lambda}, \quad (5)$$

$$V_{12+13} = f_{12+13} \frac{\hbar}{8\pi} (\hat{\sigma}_i \cdot \vec{v}) \left(\frac{1}{r} \right) e^{-r/\lambda}, \quad (6)$$

$$V_{6+7} = -f_{6+7} \frac{\hbar^2}{4\pi m_\mu c} \times [(\hat{\sigma}_1 \cdot \vec{v})(\hat{\sigma}_2 \cdot \hat{r})] \left(\frac{1}{\lambda r} + \frac{1}{r^2} \right) e^{-r/\lambda}, \quad (7)$$

$$V_{14} = f_{14} \frac{\hbar}{4\pi} [(\hat{\sigma}_1 \times \hat{\sigma}_2) \cdot \vec{v}] \left(\frac{1}{r} \right) e^{-r/\lambda}, \quad (8)$$

$$V_{15} = -f_{15} \frac{\hbar^3}{8\pi m_1 m_2 c^2} \times \{ [\hat{\sigma}_1 \cdot (\vec{v} \times \hat{r})](\hat{\sigma}_2 \cdot \hat{r}) + (\hat{\sigma}_1 \cdot \hat{r})(\hat{\sigma}_2 \cdot (\vec{v} \times \hat{r})) \} \times \left(\frac{1}{\lambda^2 r} + \frac{3}{\lambda r^2} + \frac{3}{r^3} \right) e^{-r/\lambda}, \quad (9)$$

* Email address: pchu@lanl.gov

† Email address: youngjin@lanl.gov

and the group three includes the interactions:

$$V_8 = f_8 \frac{\hbar}{4\pi c} (\hat{\sigma}_1 \cdot \vec{v})(\hat{\sigma}_2 \cdot \vec{v}) \left(\frac{1}{r}\right) e^{-r/\lambda}, \quad (10)$$

$$V_{16} = -f_{16} \frac{\hbar^2}{8\pi m_\mu c^2} \times \{[\hat{\sigma}_1 \cdot (\vec{v} \times \hat{r})](\hat{\sigma}_2 \cdot \vec{v}) + (\hat{\sigma}_1 \cdot \vec{v})[\hat{\sigma}_2 \cdot (\vec{v} \times \hat{r})]\} \times \left(\frac{1}{\lambda r} + \frac{1}{r^2}\right) e^{-r/\lambda} \quad (11)$$

where m_μ is the reduced mass of m_1 and m_2 , and λ is the interaction length. f_i 's are the coupling strengths that we measure, which can be the combination of scalar, pseudoscalar, vector and axial-vector coupling [14, 15]. All spin-dependent interactions have the potential form as $\hat{\sigma}_1 \cdot \vec{A}$, which is similar to the Zeeman interaction term of a spin with a magnetic field, $\hat{\sigma}_1 \cdot \vec{B}$ [17], indicating \vec{A} can affect a spin like an ordinary magnetic field.

Several experimental methods on various spin-dependent interactions over a broad interaction length range have been conducted, including spectroscopy, torsion-pendulum, magnetometry, parity nonconservation and electric dipole moment experiments [13, 15]. However, most experimental searches are still related to static spin-dependent interactions including V_2, V_3, V_{9+10} and V_{11} . For the group two and the group three, Yan and Snow used neutron beams to study the spin-velocity-dependent interaction (V_{12+13}) [18] and later Yan *et al.* used the relaxation of polarized ^3He to explore the same interaction in different interaction range [19]. Adelberger and Wagner also set new constraints by combining different experimental limits [20]. Piegsa and Pignol used Ramseys technique of separated oscillatory fields with a cold neutron beam to investigate V_{4+5} [21]. Haddock *et al.* applied a slow neutron polarimeter that passed transversely polarized slow neutrons by unpolarized slabs of material to set a new constraint of V_{4+5} [22]. Chu *et al.* proposed to use spin exchange relaxation-free (SERF) magnetometers to search for exotic spin-dependent interactions [17] and later set new limits on V_{4+5} [23] and V_{12+13} [24] between polarized electrons and unpolarized nucleons. Hunter *et al.* first applied polarized geoelectrons to search for long-range spin-spin interactions [25] and later expanded the idea to the velocity-dependent spin-dependent interactions [26]. Ji *et al.* proposed to use K- ^3He spin-exchange-relaxation-free (SERF) comagnetometers with SmCo_5 spin sources [27] to search for exotic spin-dependent interactions and later Ji *et al.* used K-Rb SERF comagnetometers with SmCo_5 spin sources to set new limits on spin-spin-velocity-dependent interactions [28]. Leslie *et al.* proposed to search exotic spin-dependent interactions with rare earth iron garnet test masses (dysprosium iron garnet, DyIG) [14] while the paramagnetic insulator, gadolinium gallium garnet (GGG), also has potential for spin-dependent interactions [29].

In this paper, we consider two methods, the frequency method [17, 30] and the resonance method [31] using

TABLE I. Geometry of experiment for each interactions for the frequency method. $\hat{\sigma}_1, \hat{\sigma}_2, \vec{v}, \vec{B}_{\text{eff}}, \delta r$ for different interactions.

interaction	$\hat{\sigma}_1$	$\hat{\sigma}_2$	\vec{v}	position	\vec{B}_{eff}	$\delta r(\text{mm})$
V_2	\hat{z}	\hat{z}	\hat{z}	z	\hat{z}	1
V_3	\hat{z}	\hat{z}	\hat{z}	z	\hat{z}	1
V_{4+5}	\hat{z}	0	$\hat{\phi}$	z	\hat{z}	1
V_{6+7}	\hat{z}	\hat{z}	\hat{z}	z	\hat{z}	15
V_8	\hat{z}	\hat{z}	\hat{z}	z	\hat{z}	15
V_{9+10}	\hat{z}	0	\hat{z}	z	\hat{z}	1
V_{11}	\hat{x}	\hat{y}	\hat{z}	z	\hat{x}	1
V_{12+13}	\hat{z}	0	\hat{z}	z	\hat{z}	6
V_{14}	\hat{x}	\hat{y}	\hat{z}	z	\hat{x}	15
V_{15}	\hat{z}	\hat{z}	$\hat{\phi}$	z	\hat{z}	10
V_{16}	\hat{x}	\hat{y}	\hat{y}	z	\hat{x}	10

spin-exchange optical pumping (SEOP) polarized ^3He targets [32] with unpolarized or polarized mass. The polarization of the ^3He spins using SEOP can be close to $p \approx 1$ [32]. The polarized ^3He spins can precess at the Larmor frequency $\omega_N = \gamma_3 B_0$ in a static magnetic field \vec{B}_0 where the gyromagnetic ratio $\gamma_3 = (2\pi) \times 32.4$ MHz/T. The induced magnetization of ^3He can be measured using a sensitive magnetometer with the sensitivity from 10^{-12} to 10^{-15} T. Optical pumping magnetometers (OPM) can in general reach the sensitivity of 10^{-15} T [33]. But a reduction factor should be considered due to the geometry and the interference between ^3He and OPM. So we assume a conservative sensitivity of the magnetometer at 10^{-12} T. A typical SEOP ^3He cell has a double-cell configuration as shown in Fig. 1 [32]. The top cell is a spherical pumping chamber filled with ^3He and Rb atoms. The pumping chamber is usually in an oven in order to create Rb vapor gas for optical pumping. The bottom target chamber contains only ^3He because of temperature difference between two chambers. The pressure of ^3He is at the order of 1 atm. The cell wall thickness is about 1 mm while a thinner wall about the order of $250 \mu\text{m}$ is feasible [30]. The target chamber is at the center of the \vec{B}_0 with gradient trim coils in order to optimize the relaxation time [34].

We plan to use BGO (bismuth germanate, $\text{Bi}_4\text{Ge}_3\text{O}_{12}$) as the unpolarized mass for its high nuclear density ($4.29 \times 10^{30} \text{m}^{-3}$) and small magnetic effects [35]. DyIG (dysprosium iron garnet, $\text{Dy}_3^{3+}\text{Fe}_2^{3+}\text{Fe}_3^{3+}\text{O}_{12}$) is proposed as the polarized mass which has shown the property of near-zero magnetization at the critical temperature around 220–240K and the spin density is about 10^{26}m^{-3} [14]. In the following estimation, the BGO mass is assumed to be a cube of 2 cm used in Ref. [23] and Ref. [24] and the DyIG mass is assumed to be a cylinder with the radius of 0.4 cm and the length 0.2 cm [14].

In the frequency method, the spin-dependent interac-

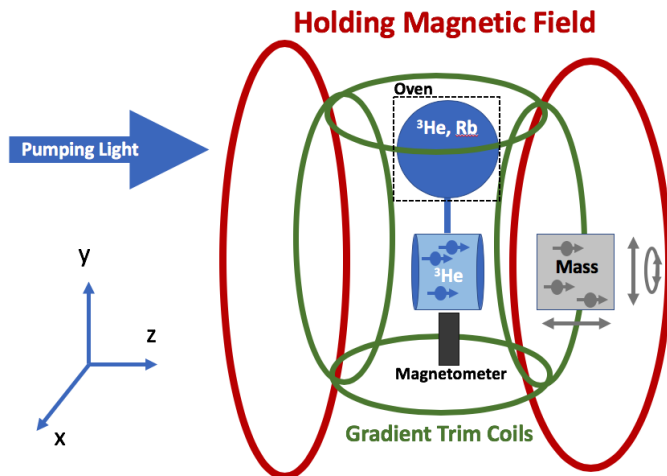


FIG. 1. The schematic of the experiment. The pumping chamber in an oven contains ^3He and Rb atoms. ^3He spins can be polarized by the pumping light through the spin-exchange with Rb electron spins. The target chamber is at the center of the holding magnetic field. Gradient trim coils are used to improve the transverse relaxation time T_2 . The mass is close to the target chamber. Using different configurations of mass motions and positions, the setup can be sensitive to different spin-dependent interactions. A sensitive magnetometer will be used to detect the magnetization of ^3He .

tions act as an effective static magnetic field \vec{B}_{eff} shifting the precession frequency. The sensitivity estimation is based on two experiments [30, 35]. Chu *et al.* [30] applied the method of gradiometers, using two pickup coils to measure different parts of the ^3He target, which have different effects from the spin-dependent interactions. In the environment without magnetic shielding, their frequency sensitivity was about 10^{-5} Hz, corresponding to $B_{\text{eff}} \sim 3 \times 10^{-13}$ T for ^3He . Tullney *et al.* [35] applied the Xe- ^3He comagnetometer in the magnetically shielded room, measuring the precession of two atomic species, which have different effects from the spin-dependent interactions. They can reach the sensitivity of 10^{-9} Hz, corresponding to $B_{\text{eff}} \sim 3 \times 10^{-17}$ T for ^3He . The practical sensitivity of B_{eff} is probably between these two values if using a magnetically shielded room with gradient trim coils. Table I shows the experimental configurations using the frequency method for each interaction. The $\hat{\sigma}_1$ means the spin orientation of the ^3He along the \vec{B}_0 . The $\hat{\sigma}_2$ means the spin orientation of the polarized mass. The \vec{v} is the velocity direction of the mass, where $\hat{\phi}$ means the rotation around the \hat{z} -axis, \hat{z} means the movement along the \hat{z} -axis, vice versa. The position means the position of the mass relative to the ^3He target chamber, where we assume the mass is always at the side to the z -axis. The direction of \vec{B}_{eff} is always along the \vec{B}_0 direction. δr means the relative minimum distance from the mass to the ^3He target chamber. $\delta r = 1$ mm means the unpolarized mass can touch the target chamber while $\delta = 5$ mm means the unpolarized mass needs to have a small distance for the

TABLE II. Parameter values used in Eq. 12.

Parameters	Symbol	Value
polarization	p	1
spin density of ^3He	n_s	$2.4 \times 10^{25} \text{ m}^{-3}$
nuclear magnetic moment of ^3He	μ_3	$-1.07 \times 10^{-26} \text{ J/T}$
gyromagnetic ratio of ^3He	γ_3	$2.03 \times 10^8 \text{ Hz/T}$
transverse relaxation time	T_2	1000 s or 53 h
sensitivity of transverse magnetization	$\mu_0 M_x$	$10^{-12} - 10^{-14} \text{ T}$
BGO nucleon density		$4.29 \times 10^{30} \text{ m}^{-3}$
DyIG spin density		$1 \times 10^{26} \text{ m}^{-3}$

TABLE III. Geometry of experiment for each interactions for the resonance method. $\hat{\sigma}_1$, $\hat{\sigma}_2$ and \vec{v} , \vec{B}_{eff} , δr for different interactions.

interaction	$\hat{\sigma}_1$	$\hat{\sigma}_2$	\vec{v}	position	\vec{B}_{eff}	δr (mm)
V_2	\hat{x}	\hat{z}	\hat{z}	z	\hat{z}	1
V_3	\hat{x}	\hat{z}	\hat{z}	z	\hat{z}	1
V_{4+5}	\hat{x}	0	$\hat{\phi}$	z	\hat{z}	1
V_{6+7}	\hat{x}	\hat{z}	\hat{z}	z	\hat{z}	15
V_8	\hat{x}	\hat{z}	\hat{z}	z	\hat{z}	15
V_{9+10}	\hat{x}	0	\hat{z}	z	\hat{z}	1
V_{11}	\hat{z}	\hat{z}	\hat{y}	z	\hat{x}	1
V_{12+13}	\hat{x}	0	\hat{z}	z	\hat{z}	6
V_{14}	\hat{z}	\hat{y}	\hat{z}	z	\hat{x}	15
V_{15}	\hat{x}	\hat{z}	$\hat{\phi}$	z	\hat{z}	10
V_{16}	\hat{z}	\hat{y}	\hat{y}	z	\hat{x}	10

velocity-dependent effect. $\delta r = 10$ mm means an additional thermal insulator thickness for the polarized mass to touch the target while $\delta r = 15$ mm means an additional distance for the velocity-dependent effect for the polarized mass. If the thermal insulator is not needed, for example, a vacuum system is applied, then δr can be reduced. Although at the critical temperature the polarized mass DyIG has zero magnetization, the temperature fluctuation could induce additional magnetic field noise. Additional magnetic shields may be necessary to reduce the magnetic effects but increase δr .

In the resonance method [31], we consider the experiment in the room temperature environment in order to simplify the experimental apparatus as a pathfinder for the low temperature experiment. The mass movement is modulated at ω_N so that the spin-dependent interactions can induce an effective oscillatory magnetic field $\vec{B}_{\text{eff}}(t) \approx \vec{B}_{\text{eff}} \cos(\omega_N t)$. The $\vec{B}_{\text{eff}}(t)$ perpendicular to the \vec{B}_0 can rotate spins from the Bloch's equation [36, 37]. The B_0 should be less than 100 nT for the precession frequency less than 3 Hz, which is feasible for most motors.

The gradiometer method can be considered, while the magnetometer method unlikely works because of different resonance frequencies between the two atomic species. The key point of the resonance method is that other magnetic field noise cannot rotate the spins as the linear oscillatory magnetic field. Therefore, the time-varying transverse magnetization M_x of ^3He [31, 36] scales linearly in response to the small B_{eff} until the measurement time $t \approx T_2$ as

$$M_x(t) \approx \frac{1}{2} p n_s \mu_3 \gamma_3 B_{\text{eff}} T_2 (e^{-t/T_1} - e^{-t/T_2}) \cos(\omega_N t) \quad (12)$$

where $n_s = 2.4 \times 10^{19} \text{cm}^{-3}$ is the spin density in the ^3He target chamber which can be calculated using the ideal gas law $PV = n_s RT$ with the pressure $P = 1 \text{ atm}$, the volume $V = 1 \text{ cm}^3$ and the room temperature $T = 300 \text{ K}$, and $\mu_3 = -2.12 \times \mu_N = -1.07 \times 10^{-26} \text{ J/T}$ is the nuclear magnetic moment of ^3He , T_1 and T_2 are the longitudinal and transverse relaxation time ($T_1 \gg T_2$). The magnetization fluctuation of ^3He [31] is $\sqrt{M_N^2} = \sqrt{\hbar \gamma_3 n_s \mu_3 T_2 / 2V} \approx 2 \times 10^{-15} \text{ T}/\mu_0$, which is at the same level of the sensitivity of the optical pumping magnetometer. However, the background noise magnetic field in a magnetically shielded room is about $10^{-15} \text{ T}/\sqrt{\text{Hz}}$. For 1 second measurement, the noise level of M_x is about $\sim 10^{-14} \text{ T}$ which can be calculated using Eq. 12 with $B_{\text{eff}} = 10^{-15} \text{ T}$ and $t = 1$, determining the sensitivity limit of M_x . Therefore, we estimate the sensitivity of $\mu_0 M_x$ about $10^{-12} - 10^{-14} \text{ T}$. If the amplitude of the transverse magnetization M_x of ^3He is $\sim 10^{-12} \text{ T}$, the worst sensitivity of the magnetometer, after 1000 s of measurement, this implies the B_{eff} upper limit is $\sim 3 \times 10^{-17} \text{ T}$. We also list the scenario with the $M_x \sim 10^{-14} \text{ T}$, the background noise limit, and the extremely long $T_2 = 53 \text{ h}$ which has been achieved in Ref. [35], giving the sensitivity of the $B_{\text{eff}} \sim 3 \times 10^{-21} \text{ T}$. The practical sensitivity is probably between $3 \times 10^{-17} \text{ T}$ and $3 \times 10^{-21} \text{ T}$. The corresponding sensitivities of SDIs can be further improved by several cycles of measurement. The corresponding parameters for Eq. 12 is summarized in Table II.

Table III shows the experimental configurations using the resonance method for each interaction. The definition of each parameter is the same as Table I. The \vec{B}_{eff} direction is always perpendicular to the \vec{B}_0 direction. For the static spin-dependent interaction such as V_2, V_3, V_{9+10} , and V_{11} , the \vec{B}_{eff} can be modulated by the distance $r(t) = r(1 + \cos(\omega_N t)) + \delta r$ so that $B_{\text{eff}}(t) \approx B_{\text{eff}}(1 + \cos(\omega_N t))$. Figure 2 shows the example of V_{9+10} . The B_{eff} is proportional to $A \equiv (\frac{1}{\lambda r} + \frac{1}{r^2})e^{-r/\lambda}$, showing spikes with the frequency equal to ω_N . The high-frequency components of $B_{\text{eff}}(t)$ larger than ω_N should be neglected, and a reduction factor should be considered when estimating the sensitivity to the B_{eff} in Eq. 12. For the spin-velocity-dependent interactions such as $V_{4+5}, V_{12+13}, V_{6+7}, V_{14}$ and V_{15} , it is straightforward to modulate the velocity such as $v(t) = v \cos(\omega_N t)$ so that $B_{\text{eff}}(t) \approx B_{\text{eff}} \cos(\omega_N t)$. Figure 3 shows the example of V_{12+13} using the same

modulation as in Fig. 2. The B_{eff} is proportional to $A \equiv (\frac{v}{r})e^{-r/\lambda}$, showing spikes with the frequency equal to ω_N . For the spin-velocity-velocity-dependent interactions such as V_8 and V_{16} , the $B_{\text{eff}}(t)$ at the resonance of ω_N can be still generated by the same modulation of the velocity as in Fig. 2. Figure 4 shows the example of V_8 and the B_{eff} is proportional $A \equiv v^2(\frac{1}{r})e^{-r/\lambda}$. However, the fast Fourier transform (FFT) of $A(t)$ implies that the reduction factor of B_{eff} is larger so that the sensitivity for the spin-velocity-velocity-dependent interactions is much weakened.

The dominant systematic uncertainty in this proposal is the magnetic impurities buried in the mass. For the spin-velocity-dependent interactions, this uncertainty can be efficiently suppressed by reversing mass moving direction with the frequency method [23, 24]. For other interactions and the resonance method, this systematic uncertainty could be mitigated with additional magnetic shields, however, which might affect the sensitivity of magnetometers [38]. The geometry of the magnetometer and the magnetic shields should be optimized.

The sensitivities of SDIs are estimated using the Monte Carlo method to average the interaction potentials in Eqs. 1–11 between ^3He spins and particles in the mass [17, 24]. In Fig. 5–7, we simply consider the B_{eff} sensitivity of $3 \times 10^{-13} \text{ T}$, $3 \times 10^{-17} \text{ T}$, and $3 \times 10^{-21} \text{ T}$ for each interaction. Most experiments worked on V_{9+10} [30, 35, 39–45] and the resonance method at room temperature has a significant opportunity to improve the current constraints and even overcome the astrophysics constraints [46]. In V_{4+5} , the only limit for the nuclear spin-dependent interaction was done using neutron beams with Ramseys technique of separated oscillating fields [21, 22]. We expect to improve the constraint with the frequency method or the resonance method. In V_{12+13} , the resonance method can also significantly improve the current constraints using neutron beams [18], the relaxation of polarized ^3He spin relaxation [19], and the combination of different experiments [20]. For spin-spin-dependent interactions, we only consider nucleon-electron interactions using polarized nuclear spins of ^3He and polarized electron spins of DyIG. In V_3 , the only constraint was done using $^8\text{Be}^+$ ion stored in Penning ion trap with polarized electron spins of a magnet [39] and the resonance method should improve the constraints. In $V_2, V_{11}, V_{6+7}, V_8, V_{14}, V_{15}, V_{16}$, the constraints between polarized nucleons and polarized electrons are rare. The only constraints were all done using the ^{199}Hg -Cs comagnetometer with polarized electron spins of Earth [25, 26] for possible long-range interactions. There is no constraint in the region of 1 m for the spin-spin-dependent interactions between nucleons and electrons. Using polarized ^3He with the frequency method or the resonance method could be the first one to explore this interaction length range.

In conclusion, we estimate the sensitivity using a polarized ^3He target with the frequency method and the resonance method [31] to search for the exotic spin-dependent

interactions for polarized nucleons. Our calculations of the projected experimental sensitivity showed that the experiments are sensitive to the interaction range of 10^{-2} to 10^{-4} m. The resonance method especially has a significant potential to improve the current constraints. However, the reduction factor should be carefully calculated

in the future for real experiments.

The authors thank P. E. Magnelind for his feedback. Research presented in this article was supported by the Laboratory Directed Research and Development program of Los Alamos National Laboratory under project number 20180129ER.

-
- [1] E. D. Commins, Annual Review of Nuclear and Particle Science **62**, 133 (2012).
- [2] J. E. Moody and F. Wilczek, Phys. Rev. D **30**, 130 (1984).
- [3] B. A. Dobrescu and I. Mocioiu, JHEP **11**, 005 (2006).
- [4] R. D. Peccei and H. R. Quinn, Phys. Rev. Lett. **38**, 1440 (1977).
- [5] L. D. Duffy and K. van Bibber, New J. Phys. **11**, 105008 (2009).
- [6] A. Arvanitaki, S. Dimopoulos, S. Dubovsky, N. Kaloper, and J. March-Russell, Phys. Rev. D **81**, 123530 (2010).
- [7] P. W. Graham, D. E. Kaplan, and S. Rajendran, Phys. Rev. Lett. **115**, 221801 (2015).
- [8] V. Flambaum, S. Lambert, and M. Pospelov, Phys. Rev. D **80**, 105021 (2009).
- [9] H. Georgi, Phys. Rev. Lett. **98**, 221601 (2007).
- [10] T. Appelquist, B. A. Dobrescu, and A. R. Hopper, Phys. Rev. D **68**, 035012 (2003).
- [11] B. A. Dobrescu, Phys. Rev. Lett. **94**, 151802 (2005).
- [12] L. Ackerman, M. R. Buckley, S. M. Carroll, and M. Kamionkowski, Phys. Rev. D **79**, 023519 (2009).
- [13] M. S. Safronova, D. Budker, D. DeMille, D. F. J. Kimball, A. Derevianko, and C. W. Clark, Rev. Mod. Phys. **90**, 025008 (2018).
- [14] T. M. Leslie, E. Weisman, R. Khatiwada, and J. C. Long, Phys. Rev. **D89**, 114022 (2014).
- [15] P. Fadeev, Y. V. Stadnik, F. Ficek, M. G. Kozlov, V. V. Flambaum, and D. Budker, Phys. Rev. **A99**, 022113 (2019).
- [16] P. Fadeev, F. Ficek, M. G. Kozlov, D. Budker, and V. V. Flambaum, (2019), arXiv:1911.05816 [hep-ph].
- [17] P.-H. Chu, Y. J. Kim, and I. Savukov, Phys. Rev. D **94**, 036002 (2016).
- [18] H. Yan and W. M. Snow, Phys. Rev. Lett. **110**, 082003 (2013), arXiv:1211.6523 [nucl-ex].
- [19] H. Yan, G. A. Sun, S. M. Peng, Y. Zhang, C. Fu, H. Guo, and B. Q. Liu, Phys. Rev. Lett. **115**, 182001 (2015).
- [20] E. G. Adelberger and T. A. Wagner, Phys. Rev. D **88**, 031101 (2013).
- [21] F. M. Piegsa and G. Pignol, Phys. Rev. Lett. **108**, 181801 (2012).
- [22] C. Haddock, J. Amadio, E. Anderson, L. Barrn-Palos, B. Crawford, C. Crawford, D. Esposito, W. Fox, I. Francis, J. Fry, and et al., Physics Letters B **783**, 227233 (2018).
- [23] Y. J. Kim, P.-H. Chu, and I. Savukov, Phys. Rev. Lett. **121**, 091802 (2018), arXiv:1702.02974 [physics.ins-det].
- [24] Y. J. Kim, P.-H. Chu, I. Savukov, and S. Newman, Nature Commun. **10**, 2245 (2019), arXiv:1902.00128 [hep-ex].
- [25] L. Hunter, J. Gordon, S. Peck, D. Ang, and J.-F. Lin, Science **339**, 928 (2013).
- [26] L. R. Hunter and D. G. Ang, Phys. Rev. Lett. **112**, 091803 (2014).
- [27] W. Ji, C. B. Fu, and H. Gao, Phys. Rev. D **95**, 075014 (2017).
- [28] W. Ji, Y. Chen, C. Fu, M. Ding, J. Fang, Z. Xiao, K. Wei, and H. Yan, Phys. Rev. Lett. **121**, 261803 (2018).
- [29] P.-H. Chu, E. Weisman, C.-Y. Liu, and J. C. Long, Phys. Rev. **D91**, 102006 (2015), arXiv:1504.00552 [hep-ph].
- [30] P. H. Chu *et al.*, Phys. Rev. **D87**, 011105 (2013).
- [31] A. Arvanitaki and A. A. Geraci, Phys. Rev. Lett. **113**, 161801 (2014), arXiv:1403.1290 [hep-ph].
- [32] T. Gentile, P. Nacher, B. Saam, and T. Walker, Reviews of Modern Physics **89** (2017), 10.1103/revmodphys.89.045004.
- [33] D. Budker and M. Romalis, Nature Physics **3**, 227234 (2007).
- [34] M. A. Rosenberry and T. E. Chupp, Phys. Rev. Lett. **86**, 22 (2001).
- [35] K. Tullney, F. Allmendinger, M. Burghoff, W. Heil, S. Karpuk, W. Kilian, S. Knappe-Grüneberg, W. Müller, U. Schmidt, A. Schnabel, F. Seifert, Y. Sobolev, and L. Trahms, Phys. Rev. Lett. **111**, 100801 (2013).
- [36] F. Bloch, Phys. Rev. **70**, 460 (1946).
- [37] P.-H. Chu and J.-C. Peng, Nucl. Instrum. Meth. **A795**, 128 (2015), arXiv:1505.06406 [nucl-ex].
- [38] S.-K. Lee and M. V. Romalis, Journal of Applied Physics **103**, 084904 (2008).
- [39] D. J. Wineland, J. J. Bollinger, D. J. Heinzen, W. M. Itano, and M. G. Raizen, Phys. Rev. Lett. **67**, 1735 (1991).
- [40] B. J. Venema, P. K. Majumder, S. K. Lamoreaux, B. R. Heckel, and E. N. Fortson, Phys. Rev. Lett. **68**, 135 (1992).
- [41] A. N. Youdin, D. Krause, Jr., K. Jagannathan, L. R. Hunter, and S. K. Lamoreaux, Phys. Rev. Lett. **77**, 2170 (1996).
- [42] A. K. Petukhov, G. Pignol, D. Jullien, and K. H. Andersen, Phys. Rev. Lett. **105**, 170401 (2010).
- [43] M. Bulatowicz, R. Griffith, M. Larsen, J. Mirijanian, C. B. Fu, E. Smith, W. M. Snow, H. Yan, and T. G. Walker, Phys. Rev. Lett. **111**, 102001 (2013).
- [44] M. Guigue, D. Jullien, A. K. Petukhov, and G. Pignol, Phys. Rev. **D92**, 114001 (2015).
- [45] J. Lee, A. Almasi, and M. Romalis, Phys. Rev. Lett. **120**, 161801 (2018), arXiv:1801.02757 [hep-ex].
- [46] G. Raffelt, Phys. Rev. **D86**, 015001 (2012).

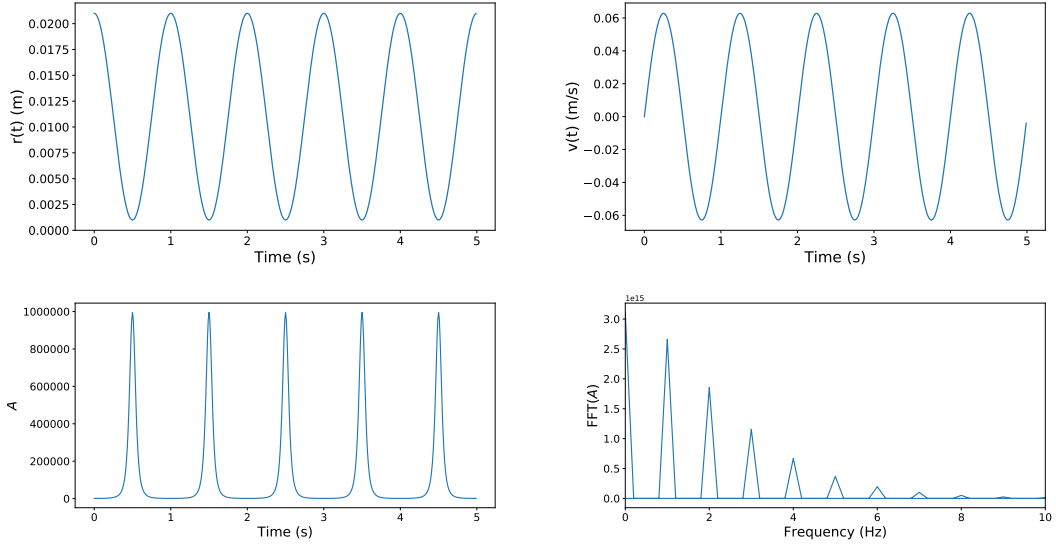


FIG. 2. The distance between the mass and the target is $r(t) = 0.01(1 + \cos(\omega_N t)) + 0.001$ and the velocity is $v(t) = 0.01\omega_N \sin(\omega_N t)$ where $\omega_N = 2\pi f_N = 2\pi \times 1$ Hz. If $\lambda = 0.01$ m, the B_{eff} due to V_{9+10} is proportional to $A \equiv (\frac{1}{\lambda r} + \frac{1}{r^2})e^{-r/\lambda}$ which is roughly a function of $\sin(\omega_N t)$. The fast Fourier transform of A is $\text{FFT}(A)$ showing the component of f_N .

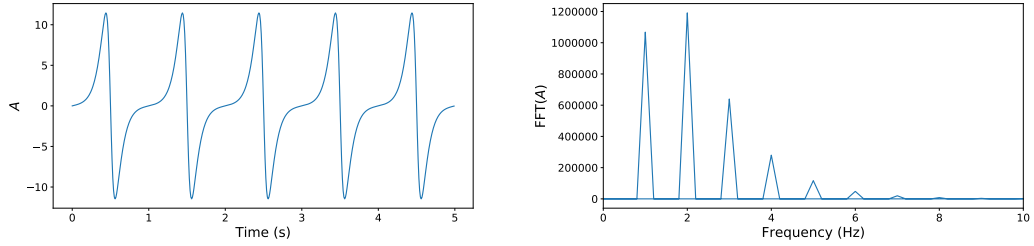


FIG. 3. If $\lambda = 0.01$ m, the B_{eff} due to V_{12+13} is proportional to $A \equiv v(\frac{1}{r})e^{-r/\lambda}$. The fast Fourier transform of A is $\text{FFT}(A)$ showing the component of f_N . The peak of $f_N = 1$ Hz is relatively weaker.

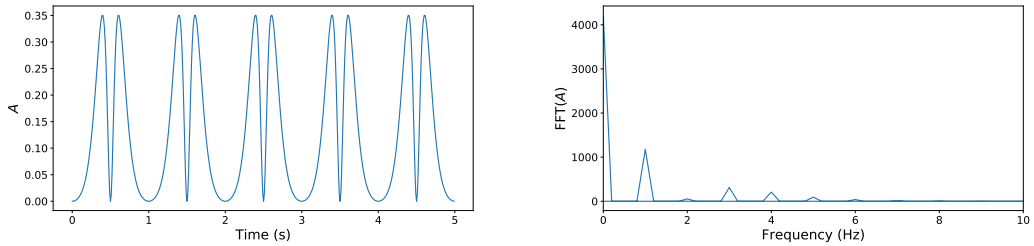


FIG. 4. If $\lambda = 0.01$ m, the B_{eff} due to V_8 is proportional to $A \equiv v^2(\frac{1}{r})e^{-r/\lambda}$. The fast Fourier transform of A is $\text{FFT}(A)$ showing the component of f_N .

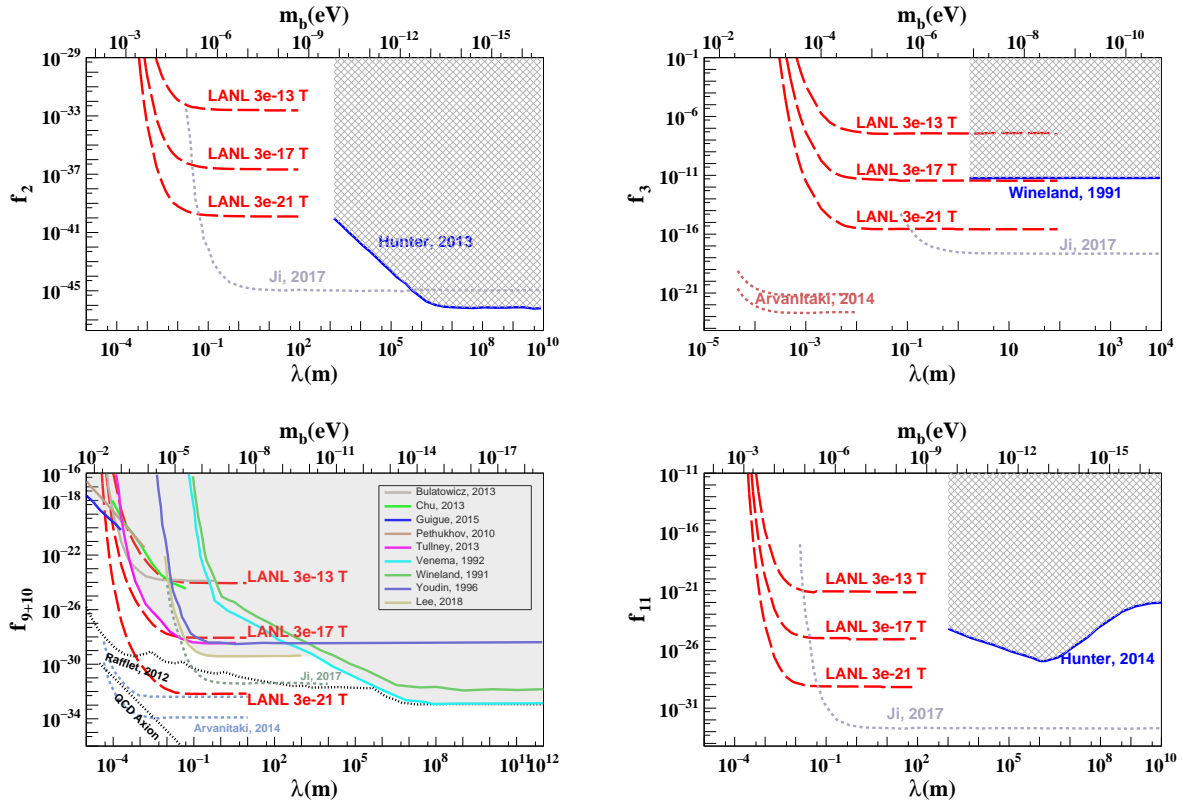


FIG. 5. The limits and the sensitivity estimation of V_2 [25, 27], V_3 [27, 31, 39], V_{9+10} [27, 30, 31, 35, 39–46], and V_{11} [25, 27].

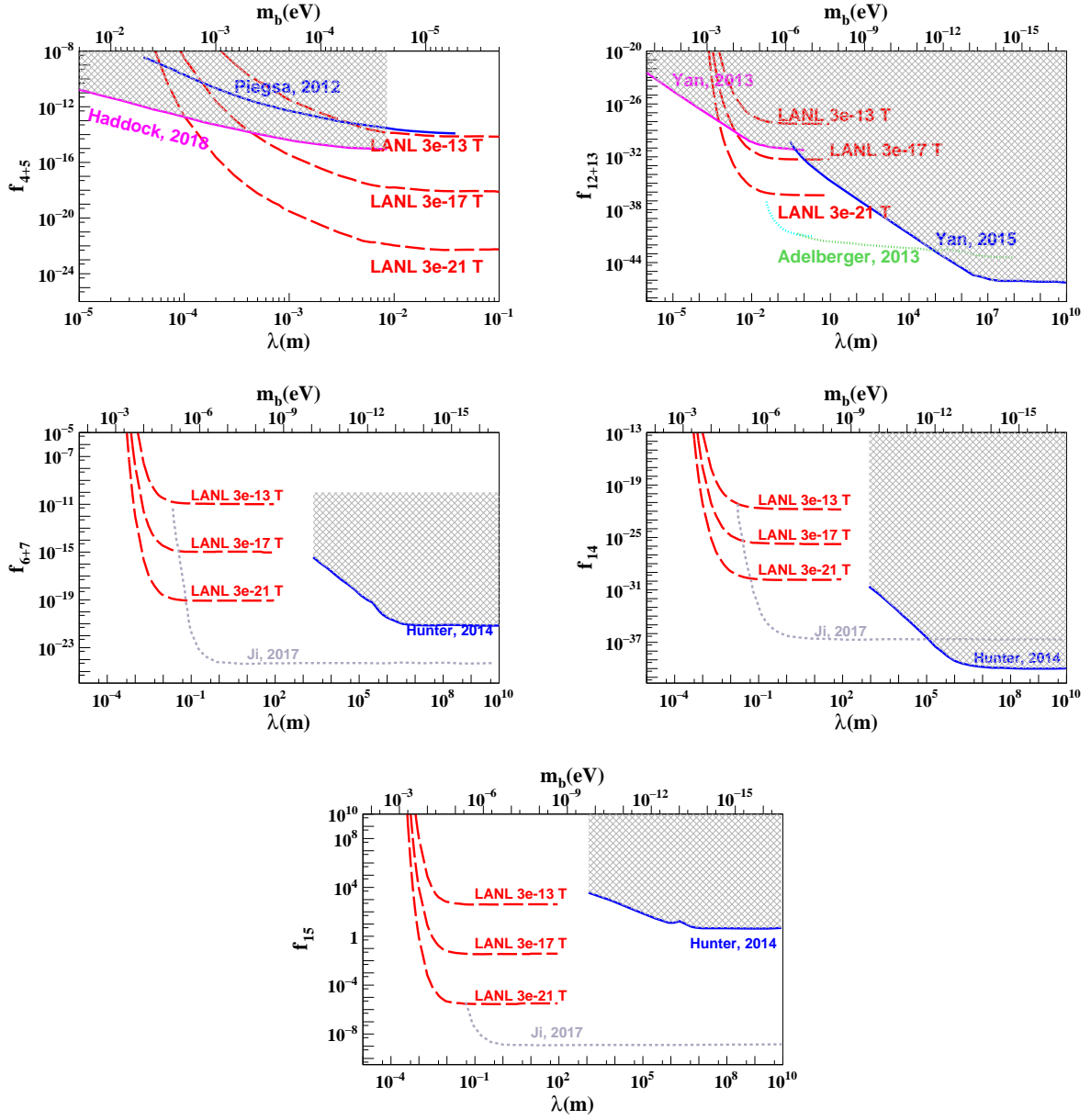


FIG. 6. The limits and the sensitivity estimation of V_{4+5} [21], V_{12+13} [18–20], V_{6+7} [26, 27], V_{14} [26, 27], and V_{15} [26, 27].

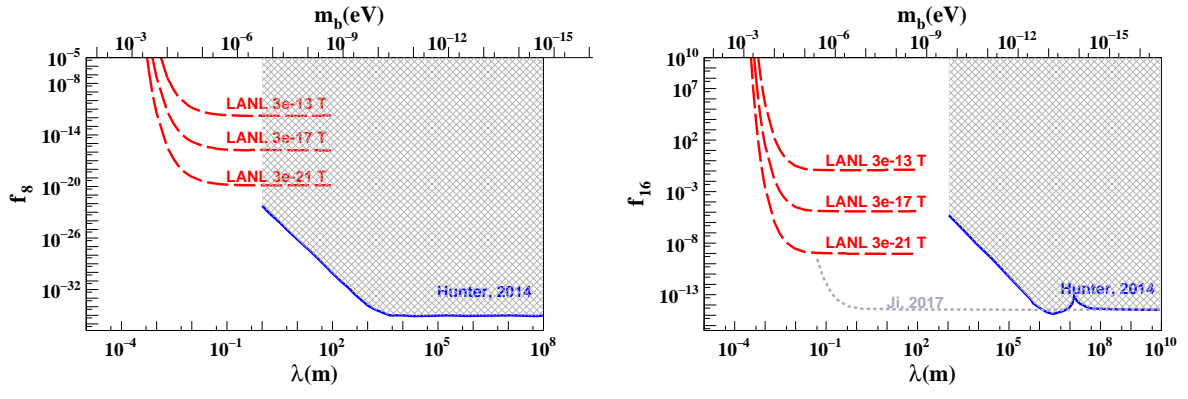


FIG. 7. The limits and the sensitivity estimation of V_8 [26], and V_{16} [26, 27].